Article

Metallic Transition Metal Dichalcogenide Nanosheets as an Effective and Biocompatible Transducer for Electrochemical Detection of Pesticide

Fengnian Zhao, Yao Yao, Xunjia Li, Lingyi Lan, Chengmei Jiang, and Jianfeng Ping

Anal. Chem., **Just Accepted Manuscript** • DOI: 10.1021/acs.analchem.8b03250 • Publication Date (Web): 29 Aug 2018

Metallic Transition Metal Dichalcogenide Nanosheets as an Effective and Biocompatible Transducer for Electrochemical Detection of Pesticide

Fengnian Zhao, Yao Yao, Xunjia Li, Lingyi Lan, Chengmei Jiang, Jianfeng Ping*

School of Biosystems Engineering and Food Science, Zhejiang University, 866 Yuhangtang Road, Hangzhou 310058, P.R. China

Corresponding author: Prof. Jianfeng Ping

E-mail: jfping@zju.edu.cn

Abstract: Owing to their large specific surface, favorable electrical conductivity, and excellent electrocatalytic capabilities, two-dimensional transition metal dichalcogenides have received considerable attention in the field of biosensor. Based on these properties, we developed a portable and disposable enzyme-based biosensor for paraoxon detection using metallic MoS_2 nanosheets modified screen-printed electrode (SPE). The exfoliated ultrathin metallic MoS_2 nanosheets can accelerate the electron transfer on electrode surface and contribute to the immobilization of acetylcholinesterase (AChE) via the cross-linking of glutaraldehyde. Electrodeposited gold nanoparticles (AuNPs) on SPE were used to immobilize MoS_2 nanosheets through the interaction between Au atoms on AuNPs and S atoms on MoS_2. Using acetylcholine as the substrate, AChE can catalyze the formation of electroactive thiocholine and further generate the redox current. In the presence of paraoxon, the activity of AChE can be inhibited, making the related electrochemical signals weaken. Under the optimized conditions, this electrochemical biosensor exhibited favorable linear relationship with the concentration of paraoxon from 1.0 to 1000 μg L^{-1}, with the detection limit of 0.013 μg L^{-1}. Furthermore, this developed biosensor was successfully applied to detect paraoxon in pretreated apple and pakchoi samples, which can provide a reliable method for the rapid analysis of organophosphorus pesticides in agricultural products.

Keywords: Enzymatic biosensor, metallic MoS_2 nanosheets, organophosphate pesticides, electrochemical biosensors, screen-printed electrode

INTRODUCTION

As the analogue of graphene, two-dimensional (2D) transition metal dichalcogenides (TMDs), such as MoS_2, WS_2, and $MoSe_2$, have raised tremendous concern given their outstanding electronic, chemical, optical, and catalytic properties since they appeared.[1,2] With the interaction of van der Waals forces, these lamellar materials are constituted by a transition metal atomic layer clamped by two chalcogen atomic layers and further stacked into multiple trilayers.[3] For TMDs, the diverse structures confer their distinguishing properties. Based on the numbers of X atoms around one M atom, MX_2 can be divided into trigonal prismatic (2H) phase and octahedral (1T) phase. As the representative TMDs, MoS_2 has a wide application in lubrication, catalysis, energy storage, and photovoltaics.[4] Currently, it has been reported that considerable metallic 1T-phase thin nanosheets from bulk MoS_2 can be obtained by some exfoliation methods, such as chemical lithium-intercalation method,[5] electrochemical lithium-intercalation exfoliation method,[4] and pressurized hydrothermal method.[7] These metallic 1T-phase thin nanosheets are of unexpected properties, such as ultrafast electronic conductivity, large surface area, and ultrahigh electrocatalytic activity, which can consequently open an avenue for their analytical detection application.[8]

Pesticides are necessary compounds in agricultural production, which play the essential role in the harvest of crops. Although they have superior effects on the prevention and control of pests and diseases, their inherent or potential toxicity and pollution for animals and environment are inevitable.[9] Organophosphorus pesticides (OPs) are a group of organic compounds, which have been widely used as insecticides and nerve agents due to their broad-spectrum and high-efficient properties, since the Second World War.[10] With the

development of research, people have realized the problem causing by the accumulation and migration of OPs, such as dichloro-diphenyl-trichloroethane (DDT), which even have caused a huge disaster. In China, some OPs (*e.g.* parathion, sulfotepp, and methamidophos) have been registered in the prohibition-restricted list of Ministry of Agriculture. Hence, it is necessary to establish an easy, rapid, and reliable analysis method for the determination of OPs.

At present, chromatographic methods, such as high-performance liquid chromatography (HPLC),[11,12] liquid chromatography-tandem mass spectrometry (LC-MS/MS),[13,14] and gas chromatography-mass spectrometry (GC-MS/MS)[15] are the most common analytical methods for pesticides at trace lever. However, these methods require the complex sample preparation and professional operators, which cannot satisfy the rapid determination at low cost. As the supplement of traditional methods, electroanalytical method is one of the most promising methods, which meets the above requirements. For most pesticides, the common electroanalytical methods mainly depend on the enzyme inhibition mechanism. Acetylcholinesterase (AChE) can catalyze the hydrolysis of the neurotransmitter named acetylcholine (ACh).[16] The basic reaction catalyzed by AChE is as follows: ACh + H_2O → choline + acetate, while choline can be further transferred into the relative electroactive compound, which can be detected by the change of current.[17] The inhibition of AChE by OPs occurs by the phosphorylation of the serine residue in the active site of the enzyme. Based on the mechanism, researchers have developed various enzyme-based electrochemical biosensors for pesticide detection.[18,19] In order to further improve the sensor performance of sensitivity and stability, graphene,[20-23] carbon nanotube,[24-26] metal or metallic nanoparticles,[27-29] and other

nanomaterials[30,31] are modified on the surface of electrode. Nowadays, there are only several researches[5,32,33] using TMDs for pesticide detection. However, the above pesticide biosensors are mainly constructed using 2H-phase MoS_2. Compared with it, 1T-phase MoS_2 possesses better electrochemical property in the field of sensing.[8]

Herein, a disposable enzyme-based pesticide biosensor using metallic MoS_2 nanosheets as the electrochemical platform was developed in this work. Due to its wide application in the growing of crops, paraoxon was selected as the model pesticide. Besides, paraoxon was the oxidization product of parathion.[34-36] Therefore, the detection of paraoxon can also reflect the residue status of parathion in a manner. The fabrication and detection process of the proposed biosensor are illustrated in **Scheme 1**. The commercial screen-printed electrode (SPE) was used as the electrode substrate. To enhance the sensor performance, AuNPs were electrochemically deposited *in situ* on the surface of SPE. Metallic MoS_2 nanosheets with high-content of 1T-phase were prepared by the chemical lithium-intercalation method. Results demonstrated that this disposable biosensor had favorable response towards paraoxon, making the low-cost, fast, and reliable determination of OPs in agricultural products come true.

EXPERIMENTAL SECTION

Chemical and Instrumentation. Molybdenum disulfide (99.9%) in this study was obtained from Graphene Laboratories Inc. (New York, USA). *N*-butyllithium solution, 1.6 M in hexane, was purchased from Macklin Inc. (Shanghai, China). Paraoxon was purchased from Dr Ehrenstorfer GmbH (Augsburg, Germany). Acetylcholinesterase (AChE) from *electrophorus electricus*, acetylthiocholine iodide (ATChI), glutaraldehyde (GA, 50%), bovine serum albumin (BSA), and gold(III) chloride trihydrate were bought from

Sigma-Aldrich (St. Louis, Mo, USA). AChE was dissolved in 1.0% BSA (w/v) for storage.[18] Methanol, hexane, and other chemical reagents were all of the analytical grade, which were purchased from the Chemical Reagent Company (Beijing, China). Primary secondary amine (PSA) and octadecyl-modified silica (C_{18}) were purchased from Agela Technologies (Tianjin, China). Phosphate buffer solution (PBS, pH 7.4) from Sangon Biotech (Shanghai, China) was diluted into 0.01 M before use. Ultra-pure water was used in this experiment via a Milli-Q purification system (Millipore, MA, USA). Three electrode SPE was bought from Zensor R&d Co. (Taiwan, China). Fresh apple and pakchoi samples were purchased from the local supermarket (Hangzhou, China). Electrochemical experiments were operated with a CHI 760E electrochemical workstation (Shanghai CH Instruments, China) at the room temperature. Inductively coupled plasma mass spectrometry (ICP-MS) machine (ELAN DRC-e, PerkinElmer, USA) was used to analyze the concentration of MoS_2. Transmission electron microscopy (TEM) images were collected via a transmission electron microscope (Tecnai G2 F20 S-TWIN, USA). Atomic force microscopy (AFM) images were obtained via the Dimension Icon AFM (Bruker AXS, Germany) in tapping mode under ambient conditions. Scanning electron microscopy (SEM) images were gained by a field emission scanning electron microscope (HITACHI-SU8010, Japan). Raman spectroscopy was collected through a LabRAM HR Evolution Raman microscope system (Horiba Jobin Yvon, Kyoto). X-ray photoelectron spectroscopy (XPS) measurements were evaluated by the AXIS Supra spectrometer (Kratos, UK).

Synthesis of Metallic MoS_2 Nanosheets. Chemical lithium-intercalation method was used to prepare the ultrathin metallic MoS_2 nanosheets from the bulk MoS_2 powder. Briefly, 0.5 g

of MoS_2 bulk powder was dispersed in 5.0 mL of 1.6 M *N*-butyllithium solution. Then, the mixture was stirred for 48 h to intercalate with lithium under argon atmosphere. After that, the processed material was separated by vacuum filtration and washed with hexane thoroughly. The obtained Li-intercalated material was then placed in 100 mL of water with ultrasonication for 60 min in ice water. The prepared suspension was first disposed with low-speed centrifugation (2,000 rpm) for 20 min to remove any unexfoliated material. Afterwards, the supernatant was gathered and then disposed with the centrifugation at 7,000 rpm for 20 min. The eventual sediment was kept in moderate ultra-pure water at 4 ℃ for further experiment. With the measurement of ICP-MS, the concentration of the final exfoliated material was 0.184 mg mL^{-1}.

To obtain semiconductive MoS_2 (2H-phase) nanosheets, the Li-intercalated material was first annealed at 300 ℃ for 2 h in the atmosphere of Ar/H_2. After that, the obtained product was dispersed in 100 mL water with ultrasonication for 60 min in ice water. The remaining steps were the same as that of metallic MoS_2 nanosheets.

Preparation of Enzyme-based Biosensor. Before the preparation, the bare SPE was activated in an ultrasonic bath with ultra-pure water for 1 min. To enhance the performance, bare SPE was firstly modified with AuNPs (denoted as SPE/AuNPs) by soaking in 1.0% $HAuCl_4$ using chronoamperometry method. Subsequently, 10 μL of exfoliated MoS_2 suspension was dropped on the surface of SPE/AuNPs (denoted as SPE/AuNPs/MoS_2) and dried at room temperature. 10 μL of 0.25% GA (diluted with ultrapure water) was coated onto the SPE/AuNPs/MoS_2 surface (denoted as SPE/AuNPs/MoS_2/GA). Finally, 10 μL of AChE (0.2 U μL^{-1}) in 5.0% BSA (1:1) was coated on the surface of modified SPE (denoted as

SPE/AuNPs/MoS_2/GA/AChE+BSA). The prepared biosensors were dried at 35 °C between each step for 30 min.

Determination of Paraoxon. In this study, the amperometric method was used for the determination of paraoxon. Before the analysis, some experimental parameters, such as the potential, inhibition time, and substrate (acetylthiocholine, ATCh) concentration were optimized to obtain the best current response. To optimize the applied potential, the CV method was adopted under the potential from –0.05 V to +0.2 V in 0.01 M PBS solution. To optimize the inhibition time and substrate concentration, the amperometric *i-t* curves were obtained before and after the addition of 50 μg L^{-1} paraoxon under the optimized potential in 0.01 M PBS solution (pH 7.4) containing certain concentration of ATCh.

Based on the catalytic mechanism, the activity of AChE can be reflected from the relative current change after the formation of the electroactive thiocholine. The following formula can express the relationship between the current and AChE activity, where t means the relative time, and ΔI means the current variation value.

$$\Delta I = \int_o^t activity \, \mathrm{dt}$$

Due to the inhibition of paraoxon, the inhibition ratio was linearly corresponding to the concentration of paraoxon. Here, we can use the following formula to calculate the inhibition ratio:

$$I\,(\%) = (\Delta I_0 - \Delta I_1) \div \Delta I_0 \times 100\%$$

where I is the inhibition percentage, ΔI_0 is the initial current in the absence of pesticide, and ΔI_1 is the final current in the presence of pesticide.

Pretreatments of Samples. The apple and pakchoi samples were cut into pieces and then

crushed via a blender, respectively. The known concentration of paraoxon was added into the obtained samples for 3 h at room temperature. After that, the prepared samples (5.0 g) were added into the centrifuge tubes containing 20 mL of 0.01 M PBS (pH 7.4) and then centrifuged for 10 min (10,000 rpm). In order to remove the organic acid, sugar, fat, and other impurities, 1.0 mL of supernatant was purified with 25 mg of PSA and 25 mg of C_{18} and vortex mixed for 1 min. The obtained mixtures were then centrifuged for 10 min (5,000 rpm). The final supernatant was filtered through a 0.22 μm filter membrane and collected as the extraction solution for the further analysis.

In order to analysis the pesticide residue in real samples, calibration curve was applied in this study. Parallel test was adopted to make sure the accuracy and precision for each data point.

RESULTS AND DISCUSSION

Characterization of the Exfoliated MoS_2 Nanosheets. In this study, TEM, AFM, Raman, and XPS were used to assess the morphology and chemical composition of the prepared materials, respectively (**Figure 1**). Both TEM image (**Figure 1a**) and AFM imagine (**Figure 1a**) proved that the exfoliated materials were typical nanosheets with the size of about 500 nm. From the selected area electron diffraction (SAED) pattern (top inset in **Figure 1a**), the hexagonal symmetry of MoS_2 could be observed distinctly. Moreover, the scanning transmission electron microscopy (STEM) image (bottom insert in **Figure 1a**) revealed the dominant presence of 1T-phase Mo atoms. In this work, the thickness of nanosheets was also studied. As showed in **Figure 1b** (insert), the thickness of prepared MoS_2 nanosheets is about 1.8 nm, indicating that the exfoliated nanosheets are ultrathin. Raman spectroscopy was then

employed to analyze the atomic structural arrangement of MoS_2. According to the research,[5] four main Raman peaks (J_1, J_2, E^1_g, and J_3 peaks) and two main Raman modes (the in-plane mode E^1_{2g} and the out-of-plane mode A_{1g}) were both regarded as the distinctive peaks of 1T-phased MoS_2. According to **Figure 1c**, the Raman spectrogram of our prepared metallic MoS_2 nanosheets has the distinctive peak of E^1_g and J_3 compared with that of bulk MoS_2 powder, which proved the presence of 1T-phase MoS_2. XPS spectra was used to analyze the surface elemental composition and bonding interactions of exfoliated MoS_2. The high resolution spectra of the deconvoluted peaks for Mo 3d was shown in **Figure 1d**. The bonding modes of $3d_{5/2}$ and $3d_{3/2}$ were used for the analysis of molybdenum. Two distinct pairs of peaks were observed, which were recorded as the 1T (red curve) and 2H (green curve) components, respectively. After calculation of the deconvolutions, the content of 1T-phase in the exfoliated MoS_2 nanosheets was nearly 65%, which further proved the successful exfoliation of metallic MoS_2 nanosheets in this study.

Characterization of the Prepared Biosensor. Scheme 1 summarized the fabrication process of metallic MoS_2 nanosheets-based pesticide biosensor. Frist of all, SEM images were used to characterize the morphology of AuNPs and MoS_2 nanomaterials on the surface of SPE. After the electrochemical reduction under the potential of –0.66 V with the run time of 60 s in 1.0% $HAuCl_4$ solution, AuNPs were successfully deposited on the SPE surface with the mean particle size of 100 nm (**Figure 2a**). Through the drop coating method, the prepared metallic MoS_2 nanosheets were well covered on the layer of AuNPs (**Figure 2b**), which could offer a platform for the immobilization of AChE and accelerate the electron transfer. CV and electrochemical impedance spectroscopy (EIS) were carried out in 0.1 M KCl solution

containing 5.0 mM $K_3[Fe(CN)_6]$ to assess the performance of the modified SPE. For CV measurements, the potential range was set from 0 to +0.5 V with the scan rate of 0.1 V s^{-1}. **Figure 2c** shows that the electrical conductivity of bare SPE can be well improved after the modification of metallic MoS_2 nanosheets (red line), indicating the favorable conductivity and catalytic activity of metallic MoS_2. Under the cross-linking of GA, AChE was successfully immobilized on the surface of SPE, which appeared a decreased reduction peak current (yellow line). **Figure 2d** displays the EIS curves obtained at bare SPE and the different modified layer of SPE in 0.1 M KCl solution containing 5.0 mM $K_3[Fe(CN)_6]$. Randles equivalent circuit model was chosen to fit the experimental data (inset in **Figure 2d**), where R_s, R_{ct}, C_{dl}, and Z_W were representing electrolyte resistance, charge transfer resistance, double layer capacitance, and Warburg impedance, respectively. The semicircles diameters of the EIS curves reveal that the charge transfer resistance of the nanocomposites of AuNPs and MoS_2 at the electrode-electrolyte interface (pink line) is lower than that of bare SPE and SPE/MoS_2. After the loading of AChE, the corresponding EIS curve is higher, proving the successful immobilization of enzyme. These results are consistent with the CV measurement results. To further prove the superiority of metallic MoS_2 (1T-phase dominated) nanosheets, the sensing performance of metallic MoS_2 was compared with that of semiconductive MoS_2 (2H-phase) nanosheets. From **Figure S1a** (**Supporting Information**), the peak current response of metallic MoS_2 modified SPE is higher than that of semiconductive MoS_2 modified SPE. The semicircles diameters of the EIS curves (**Figure S1b**) reveal that the charge transfer resistance of metallic MoS_2 modified SPE is much lower than that of semiconductive MoS_2 modified SPE. These results demonstrate that the metallic MoS_2 nanosheets possess much better

sensing performance than semiconductive MoS_2 nanosheets.

Amperometric Detection of Paraoxon. As described above, ATCh can be catalyzed by AChE to produce electroactive thiocholine, which can be further detected through the amperometric method. In the presence of paraoxon, the activity of AChE can be inhibited, leading to a weaker current. Before the detection of paraoxon, the experimental conditions, such as potential, ATCh concentration, and inhibition time were optimized. By the CV scanning from –0.05 V to +0.2 V in 0.01 M PBS (**Figure S2, Supporting Information**), a small anodic peak appeared at 0.12 V for SPE/AuNPs/MoS_2 compared with those obtained at bare SPE and SPE/AuNPs in the presence of ATCh, indicating the strong catalytical reaction occurred at this point. Besides, it was clear that ATCh can remarkably enhance the current intensity of the biosensor compared with the biosensor in blank PBS (blue line). In order to avoid the hydrogen-evolution reaction and obtain the best current signal, the low potential of 0.12 V was applied for the next amperometric studies.

The inhibition time and ATCh concentration were also studied to ensure the optimum working capacity for AChE. The prepared enzyme-based biosensor was soaked into 0.01 M PBS containing 50 μg L^{-1} paraoxon for 5, 10, 15, 20, and 30 min, respectively. As shown in **Figure S3a** (**Supporting Information**), the inhibition rate tended to be saturated after 15 min. Considering the short time consumption for rapid detection, we selected 15 min as the optimized inhibition time. A series of ATCh concentrations (50, 100, 250, 500, 1000 μM) were also set to obtain the optimized inhibition rate for paraoxon. From **Figure S3b** (**Supporting Information**), the inhibition rate is increased with the increase of AChE concentration. As a result, 500 μM was chosen as the optimized substrate concentration due to

its high inhibition rate.

In addition, the electrocatalytic activity of the prepared biosensor was tested by the injection of 500 μM ATCh under the potential of 0.12 V. **Figure 3** shows that there is no current response at bare SPE. The small increase in the current response appeared with the injection of ATCh, after the modification of AuNPs and MoS_2 on the SPE. Maybe it was due to the existence of iodide counterions or the catalysis of MoS_2 when ATCh used. Interestingly, after the modification of AChE, the current response of SPE/AuNPs/MoS_2/GA/AChE+BSA was significantly enhanced compared with that of SPE/AuNPs/GA/AChE+BSA in the presence of ATCh, indicating the metallic MoS_2 nanosheets would accelerate the catalytic efficiency of AChE.

Based on the above optimized parameters, the amperometric detection of paraoxon was carried out by immersing the proposed biosensor in stirred 0.01 M PBS with the addition of paraoxon for 15 min. As shown in **Figure 4a**, the corresponding current intensity was decreased with the addition of paraoxon from 1.0 to 1000 μg L^{-1} (*i.e.* 3.6–3634 nM in mol representation). The linear regression equation for this relationship was $I = 29.198 \lg C + 3.5798$ ($R^2 = 0.9920$), where I is the inhibition rate and C is the concentration of paraoxon. By using the equation of detection limit (LOD) = 3 Sb/m (Sb is the standard deviation of the *i-t* current in blank of pesticide and m is the slope of the calibration graph), the LOD was calculated to be 0.013 μg L^{-1} (*i.e.* 0.04 nM in mol representation) for paraoxon, proving the proposed biosensor was quite sensitive. The properties of this biosensor were also compared with the previous researches, which were listed in **Table S1**. It can be seen that our developed biosensor possesses better analytical performance with other reported pesticide sensors.

Interference Study. In order to verify the adaptation in the complex matrix, selectivity study has been carried out in the presence of in various interferences, including phenol, ascorbic acid, Ca^{2+}, Mg^{2+}, Zn^{2+}, and Cd^{2+}. As given in **Figure 4b**, phenol, Ca^{2+}, Mg^{2+}, Zn^{2+}, and Cd^{2+} caused the negligible current change in the addition of ATCh, which means that our prepared biosensor exhibits favorable selectivity towards the target. Unfortunately, the current changed clearly in the presence of ascorbic acid, which was due to the pH change caused by ascorbic acid.

Real Sample Analysis. To evaluate the practical application of this fabricated biosensor, the residue of paraoxon in real samples was analysed in this study. According to Commision decision 2002/657/EC,[37] the recovery experiment was carried out with the addition of paraoxon at the spiking level of 20, 40, and 100 μg L^{-1} in blank apple and pakchoi samples. As summarized in **Table 1**, the recoveries of analyte in apple and pakchoi samples are from 84.68% to 112.83%. After three parallel experiments, the relative standard deviations (RSDs) are from 1.59% to 9.55%. These results prove that the established biosensor was of favorable precision and reliability, which can satisfy the determination of paraoxon in agricultural products.

CONCLUSIONS

In this study, a portable and disposable AChE-based biosensor using metallic MoS_2 nanosheets as the platform for paraoxon detection was prepared. It was demonstrated that the exfoliated thin-layer metallic MoS_2 nanosheets showed favorable electron transitivity and satisfactory immobilization effect for AChE. Using ATCh as the substrate, this biosensor exhibited excellent electrocatalytic activity towards the electrochemical oxidation of

thiocholine. Results demonstrate that the prepared biosensor possesses excellent linearity with the concentration of paraoxon from 1.0 to 1000 μg L^{-1}, and a low LOD of 0.013 μg L^{-1}. This metallic MoS_2 nanosheets-based pesticide biosensor is sensitive, selective, and reliable, which offers a promising way for the analysis of OPs in agricultural products.

ASSOCIATED CONTENT

Supporting Information

Three figures showing CV and EIS of semiconductive MoS_2 (2H phase) and metallic MoS_2 (1T-phase dominated) modified SPE in 0.1 M KCl solution containing 5.0 mM $K_3[Fe(CN)_6]$, CV response of bare SPE, SPE/AuNPs, and SPE/AuNPs/MoS_2 with/without the addition of 500 μM ATCh, and optimization of paraoxon inhibition time and ATCh concentration; One table listing comparison of different sensors for the detection of organophosphorus pesticides.

AUTHOR INFORMATION

Corresponding Author

***E-mail: jfping@zju.edu.cn.**

ORCID

Jianfeng Ping: 0000-0002-0579-9830

Notes

The authors declare no competing financial interest.

ACKNOWLEDGEMENT

This work was supported by the National Key Research and Development Program of China (No. 2017YFF0211300).

REFERENCES

(1) Li, H.; Qi, X. Y.; Wu, J.; Zeng, Z. Y.; Wei, J.; Zhang, H. *ACS Nano* **2013**, *7* (3), 2842-2849.

(2) Li, H.; Wu, J.; Yin, Z. Y.; Zhang, H. *Acc. Chem. Res.* **2014**, *47* (4), 1067-1075.

(3) Li, B. L.; Wang, J. P.; Zou, H. L.; Garaj, S.; Lim, C. T.; Xie, J. P.; Li, N. B.; Leong, D. T. *Adv. Funct. Mater.* **2016**, *26* (39), 7034-7056.

(4) He, P. L.; Li, H. Y.; Liu, H. L.; Wang, X. *ChemNanoMat* **2016**, *2* (7), 665-670.

(5) Nasir, M. Z. M.; Mayorga-Martinez, C. C.; Sofer, Z.; Pumera, M. *ACS Nano* **2017**, *11* (6), 5774-5784.

(6) Ejigu, A.; Kinloch, I. A.; Prestat, E.; Dryfe, R. A. W. *J. Mater. Chem. A* **2017**, *5* (22), 11316-11330.

(7) Geng, X.; Sun, W.; Wu, W.; Chen, B.; Al-Hilo, A.; Benamara, M.; Zhu, H.; Watanabe, F.; Cui, J.; Chen, T. P. *Nat. Commun.* **2016**, *7*, 10672.

(8) Ping, J. F.; Fan, Z. X.; Sindoro, M.; Ying, Y. B.; Zhang, H. *Adv. Funct. Mater.* **2017**, *27* (19), 1605817.

(9) Mostafalou, S.; Abdollahi, M. *Arch. Toxicol.* **2017**, *91* (2), 549-599.

(10) John, E. M.; Shaike, J. M. *Environ. Chem. Lett.* **2015**, *13* (3), 269-291.

(11) Rejczak, T.; Tuzimski, T. *Food Chem.* **2017**, *217*, 225-233.

(12) Liu, D. B.; Chen, W. W.; Wei, J. H.; Li, X. B.; Wang, Z.; Jiang, X. Y. *Anal. Biochem.* **2012**, *84* (9), 4185-4191.

(13) Attallah, E. R.; Amer, M. E.; Gomaa, A. M.; El Gohary, A. A. *J. Appl. Sci. Res.* **2012**, *8* (12), 5690-5697.

(14) Wang, J. J.; Gong, Z. G.; Zhang, T. T.; Feng, S.; Wang, J. D.; Zhang, Y. *J. Sep. Sci.* **2017**, *40* (11), 2398-2405.

(15) Shamsipur, M.; Yazdanfar, N.; Ghambarian, M. *Food Chem.* **2016**, *204*, 289-297.

(16) Miao, Y. Q.; He, N. Y.; Zhu, J. J. *Chem. Rev.* **2010**, *110* (9), 5216-5234.

(17) Zhang, W. Y.; Asiri, A. M.; Liu, D. L.; Du, D.; Lin, Y. H. *TrAC Trends Anal. Chem.* **2014**, *54*, 1-10.

(18) Zheng, Q. Q.; Yu, Y. H.; Fan, K.; Ji, F.; Wu, J.; Ying, Y. B. *Anal. Bioanal. Chem.* **2016**, *408* (21), 5819-5827.

(19) Tang, W.; Wu, J. *Anal. Methods* **2014**, *6* (3), 924-929.

(20) Zhang, Y.; Xia, Z.; Li, Q. Z.; Gui, G. F.; Zhao, G. Y.; Lin, L. L. *J. Electrochem. Soc.* **2017**, *164* (2), B48-B53.

(21) Guler, M.; Turkoglu, V.; Basi, Z. *Electrochim. Acta* **2017**, *240*, 129-135.

(22) Arvand, M.; Mirroshandel, A. A. *Biosens. Bioelectron.* **2017**, *96*, 324-331.

(23) Wang, H.; Zhao, G.; Chen, D. F.; Wang, Z. Q.; Liu, G. *Int. J. Electrochem. Sci.* **2016**, *11* (12), 10906-10918.

(24) Bhatt, V. D.; Joshi, S.; Becherer, M.; Lugli, P. *Sensors* **2017**, *17* (5), 1-11.

(25) Bagheri, H.; Afkhami, A.; Khoshsafar, H.; Hajian, A.; Shahriyari, A. *Biosens. Bioelectron.* **2017**, *89*, 829-836.

(26) Ye, H. X.; Guo, Z. Z.; Peng, M.; Cai, C. Y.; Chen, Y.; Cao, Y. P.; Zhang, W. Y. *Electroanalysis* **2016**, *28* (7), 1591-1596.

(27) Bao, J.; Hou, C. J.; Dong, Q. C.; Ma, X. Y.; Chen, J.; Huo, D. Q.; Yang, M.; Abd El Galil, K. H.; Chen, W.; Lei, Y. *Biosens. Bioelectron.* **2016**, *85*, 935-942.

(28) Mogha, N. K.; Sahu, V.; Sharma, M.; Sharma, R. K.; Masram, D. T. *Mater. Design* **2016**, *111*, 312-320.

(29) Zhan, H. J.; Li, J.; Liu, Z. M.; Zheng, Y. Y.; Jing, Y. F. *Anal. Methods* **2015**, *7* (9), 3903-3911.

(30) Mao, H. P.; Yan, Y. T.; Hao, N.; Liu, Q.; Qian, J.; Chen, S. B.; Wang, K. *Sens. Actuators B* **2017**, *238*, 239-248.

(31) Zhang, Q. Q.; Xu, Q. C.; Guo, Y. M.; Sun, X.; Wang, X. Y. *RSC Adv.* **2016**, *6* (29), 24698-24703.

(32) Govindasamy, M.; Chen, S. M.; Mani, V.; Akilarasan, M.; Kogularasu, S.; Subramani, B. *Microchim. Acta* **2017**, *184* (3), 725-733.

(33) Fahimi-Kashani, N.; Rashti, A.; Hormozi-Nezhad, M. R.; Mahdavi, V. *Anal. Methods* **2017**, *9* (4), 716-723.

(34) Mehta, J.; Bhardwaj, N.; Bhardwaj, S. K.; Tuteja, S. K.; Vinayak, P.; Paul, A. K.; Kim, K. H.; Deep, A. *Anal. Biochem.* **2017**, *523*, 1-9.

(35) Arduini, F.; Forchielli, M.; Amine, A.; Neagu, D.; Cacciotti, I.; Nanni, F.; Moscone, D.; Palleschi, G. *Microchim. Acta* **2015**, *182* (3-4), 643-651.

(36) Francic, N.; Bellino, M. G.; Soler-Illia, G. J.; Lobnik, A. *Analyst* **2014**, *139* (12), 3127-3136.

(37) Communities, O. J. o. t. E. *Official Journal of the European Communities* **2002**, L221-L228.

Table 1. Recovery test of paraoxon in apple and pakchoi samples.

Samples	Spiking level (μg L^{-1})	Calculated value (μg L^{-1})	Recovery (%)	RSD (%, *n*=3)
Apple	20	21.55 ± 3.21	107.76	7.47
	40	38.15 ± 2.91	95.39	1.59
	100	112.83 ± 15.65	112.83	7.17
Pakchoi	20	16.92 ± 0.73	84.62	3.46
	40	41.31 ± 3.26	103.27	3.26
	100	97.52 ± 18.33	97.52	9.55

Figure captions:

Scheme 1. Schematic illustration of the proposed pesticide biosensor. (a) electrochemical deposition of AuNPs onto SPE, (b) loading with metallic MoS_2 nanosheets, (c) crosslinking with GA, (d) immobilization of AChE and BSA on the surface of modified SPE, (e) enzymatic hydrolysis of ATCh and production of electroactive thiocholine, and (f) inhibition effect of paraoxon on AChE.

Figure 1. Characterization of ultrathin metallic MoS_2 nanosheets. (a) TEM image of MoS_2 nanosheets. Inset: (Top) Selected area electron diffraction (SAED) pattern of MoS_2 nanosheets. (Bottom) STEM image of metallic MoS_2 nanosheets. (b) AFM images of MoS_2 nanosheets (inset: highlight profile of the selected area). (c) Raman spectroscopy of bulk MoS_2 powder and metallic MoS_2 nanosheets. (d) XPS spectra of Mo 3d mode for metallic MoS_2 nanosheets.

Figure 2. SEM images of (a) AuNPs and (b) $AuNP_S/MoS_2$ composite on the surface of SPE. (c) CV and (d) EIS of each modified layer of the proposed biosensor in 0.1 M KCl solution containing 5.0 mM $K_3[Fe(CN)_6]$. For CV, the experimental conditions were as follows: scan potential is from 0 to +0.5 V, and scan rate is 0.1 V s^{-1}. For EIS, the experimental conditions were as follows: frequency ranges from 100 kHz to 0.01 Hz, and AC amplitude is 5 mV.

Figure 3. Amperometric detection with the injection of ATCh on each modified layer of the proposed biosensor in 0.01 M PBS (pH 7.4). Arrows indicate the point of injection of ATCh

(concentration of ATCh is 500 μM).

Figure 4. (a) Amperometric detection of paraoxon in 0.01 M PBS (pH 7.4) with the addition of 500 μM ATCh at 0.12 V with the incubation of 15 min (inset: calibration curve). (b) Selectivity test of the prepared biosensor in 0.01 M PBS (pH 7.4) with the addition of 500 μM ATCh at 0.12 V.

Scheme 1.

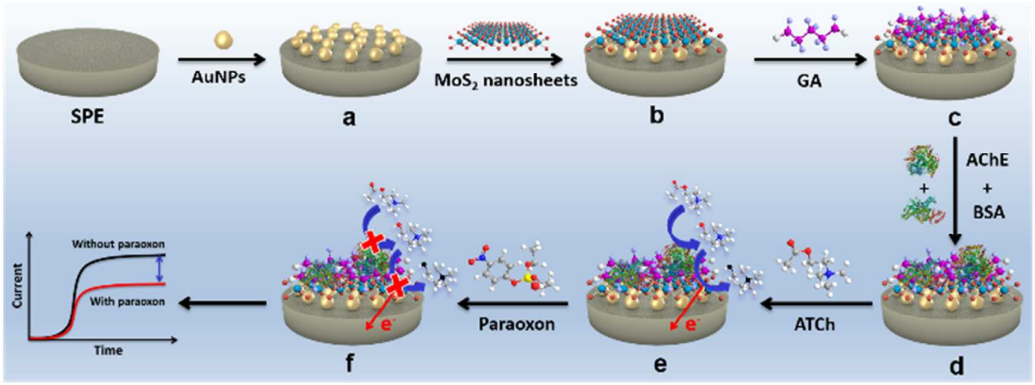
SPE
AuNPs
a
MoS2 nanosheets
b
GA
c
AChE
+
BSA
d
ATCh
e
Paraoxon
f
Without paraoxon
With paraoxon
Current
Time

414 **Figure 1.**

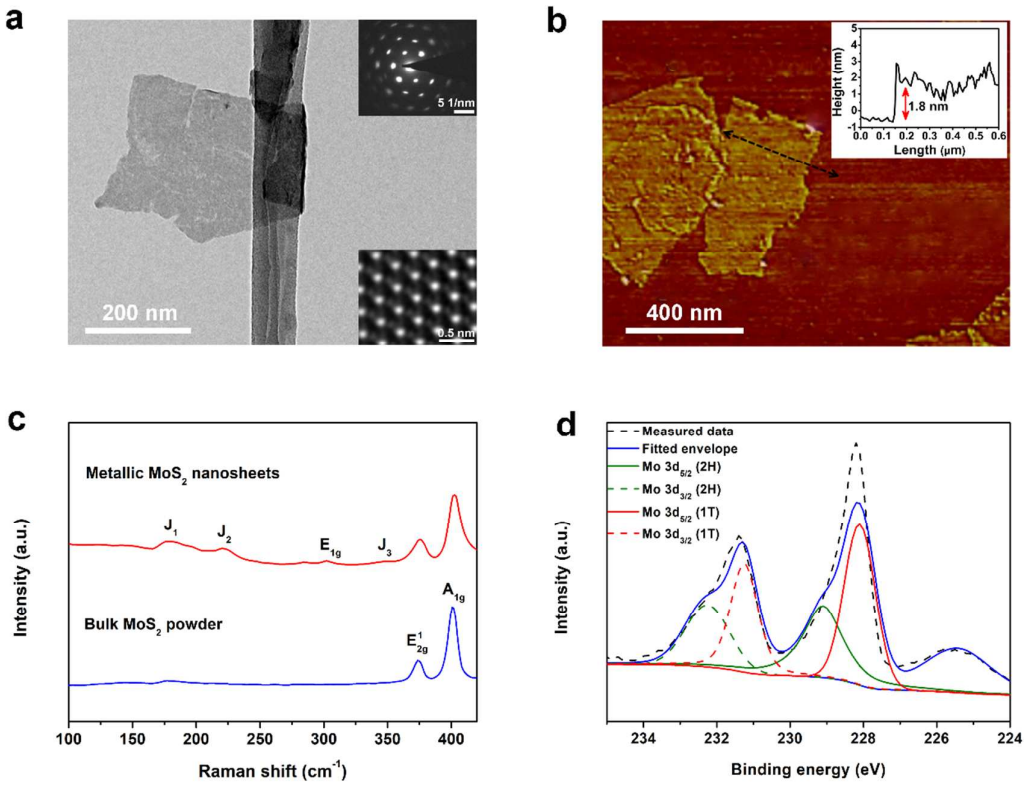

415

416

Figure 2.

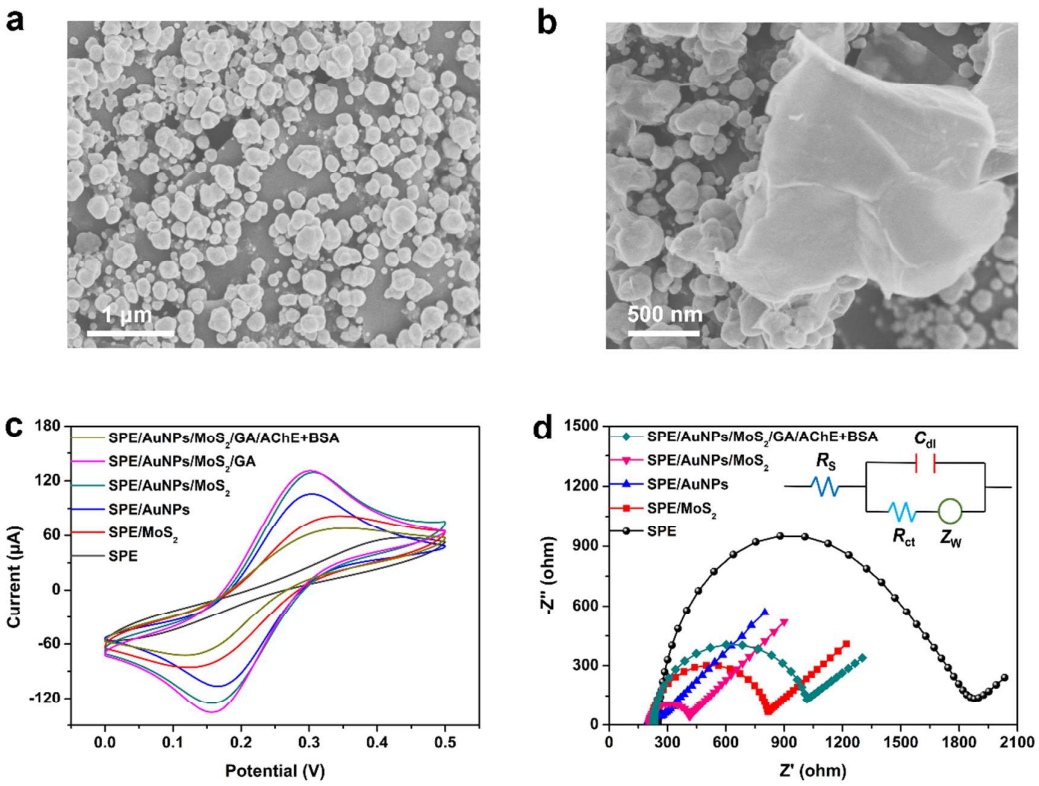
a
1 μm
b
500 nm
c
SPE/AuNPs/MoS2/GA/AChE+BSA
SPE/AuNPs/MoS2/GA
SPE/AuNPs/MoS2
SPE/AuNPs
SPE/MoS2
SPE
Current (μA)
Potential (V)
d
SPE/AuNPs/MoS2/GA/AChE+BSA
SPE/AuNPs/MoS2
SPE/AuNPs
SPE/MoS2
SPE
Cdl
RS
Rct
ZW
-Z'' (ohm)
Z' (ohm)

Figure 3.

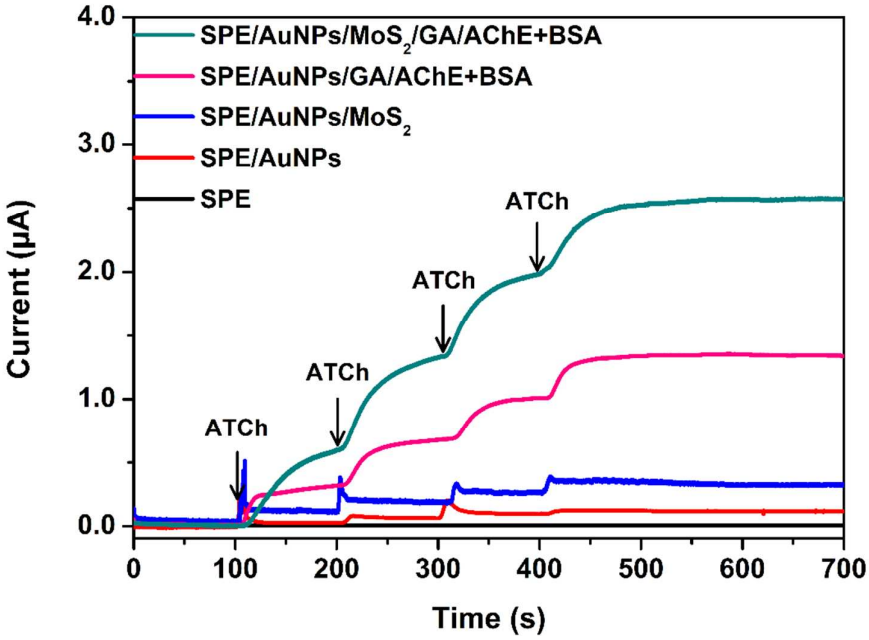
SPE/AuNPs/MoS2/GA/AChE+BSA
SPE/AuNPs/GA/AChE+BSA
SPE/AuNPs/MoS2
SPE/AuNPs
SPE
ATCh
ATCh
ATCh
ATCh
Current (μA)
Time (s)
0.0
1.0
2.0
3.0
4.0
0
100
200
300
400
500
600
700

Figure 4.

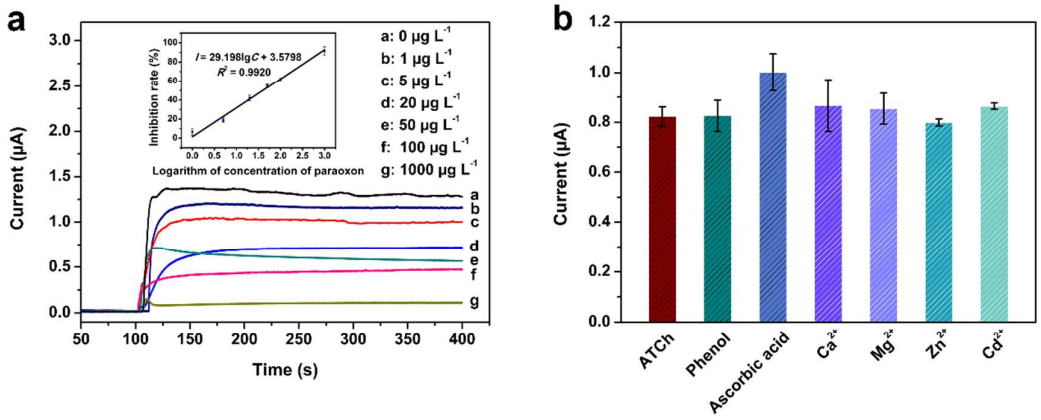
a
Current (μA)
Time (s)
Inhibition rate (%)
I = 29.198lgC + 3.5798
R² = 0.9920
Logarithm of concentration of paraoxon
a: 0 μg L⁻¹
b: 1 μg L⁻¹
c: 5 μg L⁻¹
d: 20 μg L⁻¹
e: 50 μg L⁻¹
f: 100 μg L⁻¹
g: 1000 μg L⁻¹
b
Current (μA)
ATCh
Phenol
Ascorbic acid
Ca2+
Mg2+
Zn2+
Cd2+

426 **TOC**

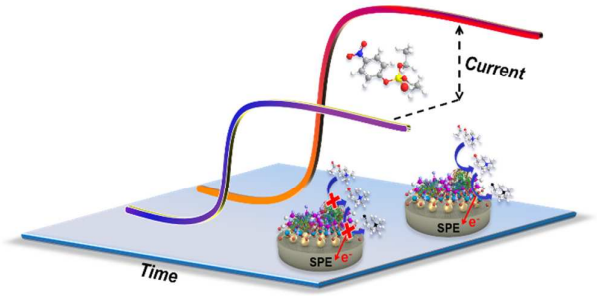

427